

Coupled electron-proton transfers and charge separation in excited-state dynamics of X-Mn-OH₂ (X=OH, OCaH) with hydrogen-bonded acceptors

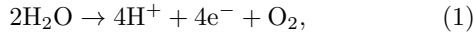
Kentaro Yamamoto^{1,*} and Kazuo Takatsuka^{1,†}

¹Department of Basic Science, Graduate School of Arts and Sciences,
The University of Tokyo, Komaba, 153-8902, Tokyo, Japan
(Dated: January 2, 2015)

We study electron dynamical mechanism of charge separation created in the excited-state reactions of molecular systems consisting of X-Mn-OH₂ ··· Ac → X-Mn-OH ··· HAc, where X = (OH, or OCaH) and Ac = (*N*-methylformamidine, guanidine, imidazole, or ammonia cluster). The roles of Ca atom are also revealed.

I. INTRODUCTION

Charge separation and recombination are of critical importance in the study of solar cells, in which photoexcited electrons emerged from an insulator are carried across an interface to a conduction band in a metal counterpart. This mechanism is however not applied to biological and organic systems in general. For instance, one of the most typical examples of charge separation is seen in an early process of photosynthesis, i.e. photo-driven water oxidation



yielding electrons and protons. It is widely recognized that this reaction is catalyzed by Mn₄CaO₅ cluster embedded in photosystem II (PSII), a membrane pigment-protein complex,¹ the dynamical mechanism of this reaction being totally an open question though.

The first X-ray crystal structure of PSII at ∼3.8 Å was published in 2001,² and in 2011 Shen and Kamiya determined the molecular structure of Mn₄CaO₅ within the resolution of 1.9 Å.¹ Since then, many theoretical studies on this cluster have been achieved; Yamaguchi and coworkers have performed systematic geometry optimization to find reaction paths.^{3–8} Siegbahn has similarly calculated energy diagram of the Kok cycle with DFT.^{9,10} Kurashige performed density matrix renormalization group calculations,¹¹ suggesting through a close examination of the spin states that the existing candidates of the structure of Mn₄CaO₅ must be reassessed.

All these studies are quite stimulating but are based on the static quantum chemical methods. By way of compensation, we study a dynamical mechanism of charge separation of water molecule. However, we here treat smaller Mn-clusters than Mn₄CaO₅, since we first aim to deduce the very basic and general mechanisms of charge separation in advance of the tougher simulation of the realistic dynamics of Mn₄CaO₅, even the molecular geometry of which is yet to be concluded as suggested by Kurashige. Besides there is no definitive information so far on in which form the photon energy absorbed in some other places is transmitted to the cluster, which should create an excited state, or possibly a state of electron attachment. Hence the electronic state (and even geometry) to be considered should be different from that of

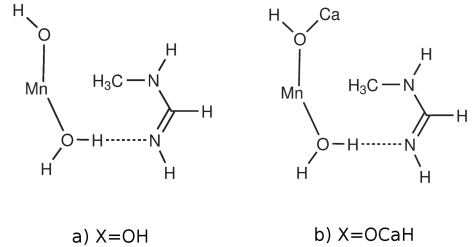


FIG. 1: Chemical structure of X-MnOH₂ ··· Ac, where Ac = *N*-methylformamidine. The structures are actually not planar, but rather twisted along the O-H ··· Ac bonds.

the stable ground state. Furthermore the charge separation is likely to be realized in the moiety of proteins and solvents, but not so directly as symbolically represented in Eq. (1). We therefore scrutinize in our simplified perspective what is the fundamental mechanism of charge separation in excited states and what are the roles of Mn and Ca atoms and amino acids nearby the clusters. To do so, we perform full-dimensional nonadiabatic electron wavepacket dynamics in the excited-state reactions of



where X = (OH or OCaH), and Ac are selected parts of amino acid residues or ammonia clusters Ac = (*N*-methylformamidine, guanidine, imidazole, or ammonia cluster). The symbols ··· and * indicate hydrogen bonding and electronically excited state, respectively. For all the various combinations between Ac and X, we have commonly identified a coupled proton and electron transfers passing through their own different pathways, thereby creating a charge separation in AcH*. Due to the space limitation, we here report only the case of Ac = *N*-methylformamidine as represented in Fig. 1.

II. SYSTEMS AND METHOD

We carry out nonadiabatic electron wavepacket dynamics in the level of theory equivalent to the semiclassical Ehrenfest theory (SET) to the first order. Here in this paper we do not consider explicit path-branching for

the sake of simplicity.^{12–16} The electron wavepacket Ψ_{elec} is expanded in the form

$$\Psi_{\text{elec}}(\mathbf{R}, \mathbf{r}, t) = \sum_I C_I(t) \Phi_I(\mathbf{r}; \mathbf{R}(t)), \quad (3)$$

along a nuclear path coordinate $\mathbf{R}(t)$, with \mathbf{r} and t being electronic and time coordinates, respectively. $C_I(t)$ are to be determined as the coefficients with respect to basis functions $\{\Phi_I(\mathbf{r}; \mathbf{R}(t))\}$ such as the Slater determinants. The dynamics of Ψ_{elec} is then reduced to the coupled equations

$$i\hbar \frac{dC_I}{dt} = \sum_J \left(H_{IJ}^{(el)} - i\hbar \sum_k \dot{R}_k X_{IJ}^k - \frac{\hbar^2}{2} \sum_k Y_{IJ}^k \right) C_J, \quad (4)$$

where $H^{(el)}$ is the electronic Hamiltonian, and $X_{IJ}^k = \langle \Phi_I | \partial \Phi_J / \partial R_k \rangle$ and $Y_{IJ}^k = \langle \Phi_I | \partial^2 \Phi_J / \partial R_k^2 \rangle$. Nuclear path $\mathbf{R}(t)$ is driven by the wavepacket-averaged force F_k defined as

$$F_k = \sum_{IJ} C_I^* \langle \Phi_I | \frac{\partial H^{(el)}}{\partial R_k} | \Phi_J \rangle C_J. \quad (5)$$

In the present paper, the second order term Y_{IJ}^k is neglected as usual, which should be justified because of the factor \hbar^2 .

In this study, these equations of motion are numerically integrated with the matrix elements calculated on-the-fly. Since the straightforward computations of SET including the derivatives of the matrix elements such as $\partial H_{IJ}^{(el)} / \partial R_k$ or X_{IJ}^k are time consuming, we have implemented a parallel computational scheme for the relevant numerical derivatives.

The basis functions for the electron wavepacket $\{\Phi_I(\mathbf{r}; \mathbf{R}(t))\}$ shown in Eq. (3) are chosen to be adiabatic wavefunctions obtained on-the-fly through quantum chemical calculations. The adiabatic wavefunctions and relevant matrix elements are calculated by using modified GAMESS package.^{17,18} We perform CISD/RHF level of calculation for all the static and dynamical analysis, except for auxiliary geometry optimization (in the RHF level). Effective core potential is adopted for Mn atom, and 6-31G basis set is for all other atoms. We added diffuse orbitals to the H and N atoms, which are crucial to describe the mechanism of electron transfer.¹⁹ Those to the other atoms have been omitted, with confirming that no qualitative difference is caused. Configuration state functions (CSFs) are generated by means of the graphical unitary group approach (GUGA).^{20,21} Only the HOMO to (HOMO+50) are taken into account to generate CSFs, and all the other molecular orbitals (MO) have been held in inactive space, since the energy gap between HOMO and HOMO-1 is quite large (commonly more than 2 eV). Also MOs higher than HOMO+51 are frozen as inactive orbitals, because the resulting low-lying adiabatic states are sufficiently converged without these higher MOs. We use the first 50 of the adiabatic states

$\{\Phi_\alpha\}$ out of 1326 in ascending order of energy as the basis set $\{\Phi_I\}$ of electron wavepacket in Eq. (3).

III. DYNAMICAL MECHANISM OF CHARGE SEPARATION

We first study excited-state electron dynamics of HO-MnOH₂ with *N*-methylformamide as in Fig. 1(a), and then a Ca atom is doped.

A. Some characteristic features of the static potential surfaces

Before a close investigation of full-dimensional dynamics, we study the basic energetics of the static potential energy surfaces. First of all, if Mn(OH)OH₂ stands alone without Ac, the Mn(OH)O(H)-H bond is stronger than the Mn(OH)-OH₂ bond. Here the hyphen “-” denotes the bonds to be compared. All the other geometries are fixed to their optimized geometry. Thus the OH bond is stronger than the MnO bond in this condition (with the potential surface not shown graphically). However, if the acceptor Ac is attached, OH bond of the water molecule is significantly weakened. Thus it is confirmed that the molecular arrangement of spin singlet in Fig. 1(a) is stable in the ground state.

Next we briefly examine the potential energy surface projected onto one-dimensional coordinate O-H···Ac (see Fig. 2(a)). We denote this H atom H^T to distinguish it from the other relatively stable H atoms. Note, however, that H^T does never imply an isolated hydrogen atom of 1s state. The H^T is confined on the line connecting O and Ac. The O-Ac length has been fixed at 2.5 Å. All the other geometries have been fixed at the initial configurations, which were energy-optimized.

The low-lying excited state S₁ and S₂ in Fig. 2(a) turn out not to lead to the transfer of H^T to the Ac side. Besides, the transition dipole between S₀ and (S₁, S₂) are both very small. (Note that the symbols S₁, S₂, and so on are not meant to be the redox states of Kok cycle.)

We therefore focus on the states S₃ and S₄, which are represented in thick lines in the figure. These excited states are accessible by photoexcitation in view of large transition dipole moments between S₀ and (S₃, S₄). We do not necessarily assume photon absorption in actual excitation process, though. The trace of the conical intersection is observed on this coordinate at R_{OH} = 1.3 Å. Indeed the nonadiabatic transition probability between S₃ and S₄ is estimated to be as large as about 0.8. In the figure we further notice that the minima of S₃ and S₄ favors a longer OH, that is, H^T is to be transferred close to Ac.

Incidentally, the one-dimensional projection of potential surfaces of the low-lying excited states for Mn₄CaO₅-OH₂ with Ac are found to be similar to those of Fig. 2(a), which will be reported elsewhere.

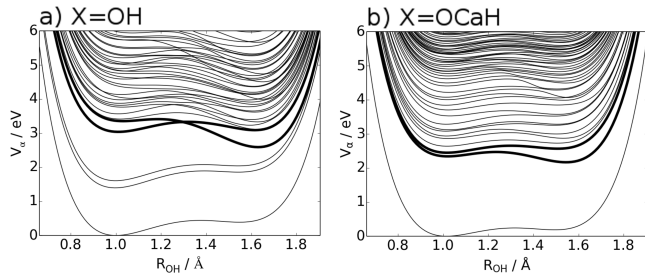


FIG. 2: One-dimensionally projected potential curves of $X\text{-MnOH}_2\cdots(N\text{-methylformamidine})$, where (a) $X=\text{OH}$ and (b) $X=\text{OCaH}$.

B. Full-dimensional electron-nuclei simultaneous dynamics

Now we perform the full-dimensional SET dynamics of $\text{HO}\text{-Mn-OH}_2\cdots(N\text{-methylformamidine})$. To choose initial conditions for nuclear positions and momenta in excited state dynamics, we beforehand had run ab initio dynamics on the S_0 state with zero-point energy. Along such classical trajectories, we picked about 20 independent points in nuclear phase space. And at each point, we lifted the electronic wavepacket up to S_4 , and began to integrate the SET dynamics. The energy allocated to H^T is as much as the barrier height located in the projected one-dimensional coordinate (see Fig. 2(a)), which is about 0.05 eV, and the total energy of nuclei is 3.7 eV. As suggested by Fig. 2(a), H^T is promptly transferred to Ac in S_4 after some bouncing motions in the short O-H region ($R_{\text{OH}} \leq 1.3\text{\AA}$).

With an illustrative example resuming S_4 dynamics at $t = 0$ fs, we below demonstrate a typical dynamics of those SET states. We first estimate how much electrons are carried by H^T by applying the hybrid method of Mulliken²² and Hirshfeld²³ atomic population analysis. As shown in Fig. 3(a), the atomic charge Q_A on H^T along the path is kept as much as +0.6. This implies that H^T is not a bare proton but dressed with 0.4 electrons.

We next investigate the radical character of the electrons on H^T . To do so, we apply the unpaired electron density $D(\mathbf{r})$, which is defined as²⁴

$$D(\mathbf{r}) = 2\rho(\mathbf{r}, \mathbf{r}) - \int d\mathbf{r}' \rho(\mathbf{r}, \mathbf{r}') \rho(\mathbf{r}', \mathbf{r}), \quad (6)$$

where $\rho(\mathbf{r}, \mathbf{r}')$ is the first order spin-less density matrix in the coordinate representation. $D(\mathbf{r})$ extracts electron density of the singly occupied orbitals and quantifies the radical character of an atom or a molecule and its spatial distribution. The population of the unpaired electrons on H^T along the reaction path is shown in Fig. 3(b). The spatial distribution of $D(\mathbf{r})$ is displayed in Fig. 4(a). The total number of the unpaired electrons is about 2.0 throughout the reaction. This indicates that the entire system is in a singlet biradical state with a distribution that is eventually (in about 10 fs) split into two pieces

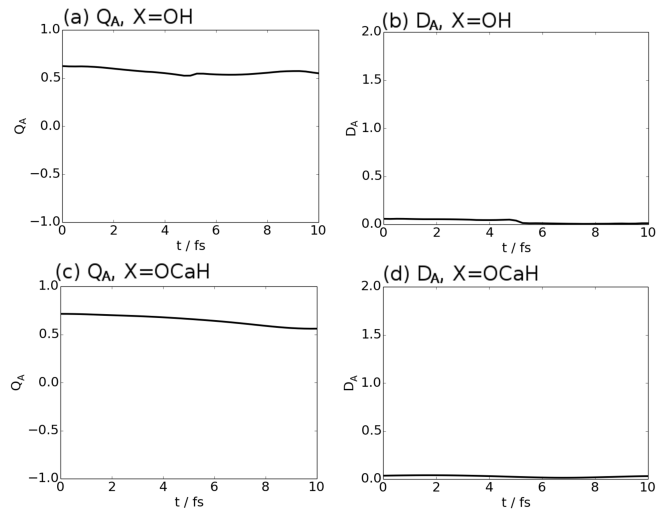


FIG. 3: (a)(c) Atomic charge Q_A on H^T along the full-dimensional SET path, which is kept as much as +0.6. (b)(d) Atomic unpaired electron density D_A on H^T along the full-dimensional SET path, which is kept close to zero.

as in the rightmost panel in Fig. 4(a)), one radical on $\text{HO}\text{-Mn-OH}$ in the ground state and the other one lying on HAc in an (asymptotically) excited state. Let us take a closer look in Fig. 4(a) at the spatial distribution of $D(\mathbf{r})$ to track the electron dynamics. In the very early stage, when H^T is in the O atom side ($\text{O-H}\cdots\text{Ac}$), most of the unpaired electrons remain on the same side. Then, when H^T takes the middle position ($\text{O}\cdots\text{H}\cdots\text{Ac}$), the unpaired electrons still stay in the middle position, but not on H^T . Therefore H^T appears not to be a radical while it is transferred, which is consistent with the values observed in Fig. 3(b). Finally, when it is transferred to Ac ($\text{O}\cdots\text{H-Ac}$), the unpaired electrons become to occupy the Rydberg-like diffused orbitals in Ac. Thus H^T does not become a radical after all and one of the radical electrons has moved onto Ac through different paths, and charge recombination is not realized in this time scale. The electrons on H^T are thus carried in a concerted manner (by one of the doubly occupied natural orbitals, although the total population on H^T is only about 0.4.) Thus one may conclude that this transfer is not hydrogen atom migration but is akin to an ordinary proton transfer in the ground state, as far as the radical character is concerned. In short, the H^T should be expressed as $\text{H}^{0.6+}$ and is not a radical throughout the process.

We next calculate the Schiff probability current of electrons (or flux, in short)²⁵ to visualize how electrons flow within the system. Electron flux analyses have been performed before by Takatsuka and coworkers,^{14,19,26–28} and Manz and coworkers,^{29,30} which have been proven to be useful to track the nuclear and/or electronic pathways. Snapshots of the electron flux shown in Fig. 5(a) indicate a circular motion of electron flow. In other words,

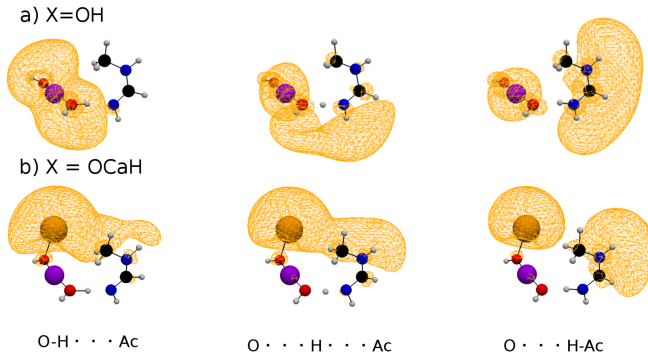


FIG. 4: Snapshots of the unpaired electron density up to about 10 fs along the SET path obtained by full-dimensional on-the-fly dynamics for the case of (a) $X=\text{OH}$ and (b) $X=\text{OCaH}$. The color indicates: H=white, C=black, N=blue, O=red, Mn=purple and Ca=orange.

the motions of electrons are not parallel to that of H^T . Initially, when H^T is on the O atom side ($\text{O}-\text{H}\cdots\text{Ac}$), relatively large electron flux can be seen only around HO-Mn-OH_2 . The unpaired electrons (Fig. 4(a)) do not move to Ac yet at this time as well. Second, when H^T takes the middle position ($\text{O}\cdots\text{H}\cdots\text{Ac}$), the electrons look moving circularly around H^T . Finally, when H^T is transferred to Ac ($\text{O}\cdots\text{H-Ac}$), the electron flux is rather pointing to the Rydberg-like diffused states than to H^T , with no hint of charge recombination either. In short, electrons are seen to jump to the Rydberg-like diffused states on Ac to induce charge separation, while H^T moves linearly from the O atom to Ac.

The entire electron dynamics is summarized as follows. The transferring proton carries only 0.4 electrons in a concerted manner, while 0.6 electrons remained is carried over onto Ac through different paths. Thus, the net charge transferred is zero. (Note that this makes a critical difference from the ground-state proton transfer, in which net one positive charge is transferred by rendering back the excess electrons sticking to the shifting proton nucleus.²⁷) After the reaction, therefore, a charge separation like a zwitter ion of +0.6 and -0.6 coexist on Ac in the present system. (Recall that reaction $\text{H}\rightarrow\text{H}^++\text{e}^-$ as in Eq. (1) needs as much as 13.6 eV to complete, which is prohibitively too high.) These charges can stay separated for a long time before charge recombination is caused by passing through a conical intersection in Ac site.

C. Dynamical roles of Ca

Stimulated by Mn_4CaO_5 embedded in PSII in natural photosynthesis, we here investigate the role of Ca atom in the present dynamics by adding Ca atom to HO-Mn-OH_2 . To the best of our knowledge, no study has been reported as to the dynamical roles of Ca atom.

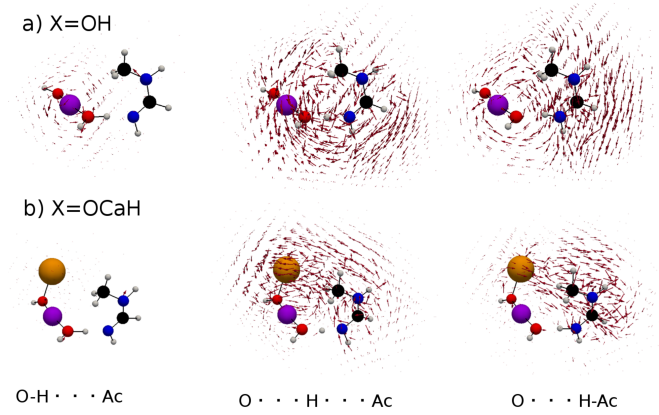


FIG. 5: Snapshots of the electron flux at the same timings as Fig. 4 along the SET path obtained by full-dimensional on-the-fly dynamics for the case of (a) $X=\text{OH}$ and (b) $X=\text{OCaH}$. The color attribution is the same as Fig. 4. Very large values coming from the inner shell electrons have been neglected for the sake of best visualization.

All the graphical analyses for the system of HCaO-Mn-OH_2 can be compared with HO-Mn-OH_2 in each figure; chemical structure in Fig. 1(b), one-dimensional projection of the potential surface in Fig. 2(b), electronic charge in Fig. 3(c) and unpaired electrons in Fig. 3(d), the spatial distribution of the unpaired electron in Fig. 4(b), and the electron flux in Fig. 5(b). As noticed, most of the features compared with HO-Mn-OH_2 are quite similar to each other, except for two important aspects: (1) The excitation energy to access the transferring excited states (expressed as thick lines in Fig. (b)) is made lowered from 3.1 eV (400 nm) to 2.4 eV (520 nm) by Ca doping. Thus the excitation energy is shifted to enter the visible light range. (2) Both the flow of the unpaired electrons and the total electron flux emerge mostly not from Mn atom but rather Ca. In the literature the role of Ca in Mn_4CaO_5 seems to be discussed only from the view point of the distorted molecular shape.¹ However, the present finding suggests more essential aspects about the role of Ca. Further analysis will be reported elsewhere.

IV. CONCLUDING REMARKS

We have investigated excited-state dynamics of $\text{X-Mn-OH}_2^*\cdots\text{Ac}\rightarrow\text{X-Mn-OH}\cdots\text{HAc}^*$ by means of the theory of nonadiabatic electron wavepacket dynamics. Various X and Ac have been examined to find a common mechanism of coupled electron-proton transfer in excited states; proton is shifted from the cluster to the amino acid residues carrying electrons as much as $(1-n)\text{e}$, with e being the elementary charge and with $n\approx 0.6$, in a concerted manner.²⁷ The remaining electrons of $n\text{e}$ flow into the Rydberg states of the amino acid residues passing through different route from that of the proton. This in-

duces charge separation composed of $+ne$ and $-ne$ in the excited state of the residues of amino acids. The similar mechanism of charge separation was first found in the $\pi - \pi^*$ transition in phenol that is hydrogen-bonded with small ammonia clusters.¹⁹ The present study suggests that this mechanism should lie indeed ubiquitously behind the phenomena of charge separation in chemical and biological systems.

The resultant proton shifted into Ac can trigger further proton-relay transfer to remote sites if the parts of amino-acid residues are replaced with appropriate proteins. Likewise electrons in the Rydberg states may be transmitted further away through the possible excited states coherently. If it happens, charge recombination is more unlikely to take place.

By comparing molecules with and without the Ca atom in the X-Mn-OH₂ systems, we have revealed that the presence of Ca atom reduces the excitation energy. Moreover, it has been observed that the excited electrons flow via the Ca atom rather than Mn.

This work is stimulated by the system of the oxygen-

evolving complex Mn₄CaO₅, which corresponds to X=Mn₃CaO₅ in the present definition. However, we do not mean to “simulate” its dynamics at this stage. Rather, we conceive that the mechanism of charge separation is not necessarily unique to Mn₄CaO₅ but should be chemically common to other similar systems. If so, one may be able to design molecules of the similar functions, and indeed the present work suggests that MnOCaH can be a candidate as such.

The relevant technical details used in this paper and path-branching dynamics of the present systems will be reported elsewhere, along with the dynamics of ion states of electron attachment on X-Mn-OH₂.

Acknowledgments

This work was supported in part by a Grant-in-Aid for Basic Science from the Ministry of Education, Culture, Sports, Science and Technology of Japan.

-
- ^{*} Electronic address: kyamamoto@mns2.c.u-tokyo.ac.jp
- [†] Electronic address: kaztak@mns2.c.u-tokyo.ac.jp
- ¹ Y. Umena, K. Kawakami, J.-R. Shen, and N. Kamiya, *Nature* **473**, 55 (2011).
- ² A. Zouni, H.-T. Witt, J. Kern, P. Fromme, N. Krauss, W. Saenger, and P. Orth, *Nature* **409**, 739 (2001).
- ³ T. Saito, S. Yamanaka, K. Kanda, H. Isobe, Y. Takano, Y. Shigeta, Y. Umena, K. Kawakami, J.-R. Shen, N. Kamiya, M. Okumura, M. Shoji, Y. Yoshioka, and K. Yamaguchi, *Int. J. Quantum Chem.* **112**, 253 (2012).
- ⁴ S. Yamanaka, T. Saito, K. Kanda, H. Isobe, Y. Umena, K. Kawakami, J.-R. Shen, N. Kamiya, M. Okumura, H. Nakamura, and K. Yamaguchi, *Int. J. Quantum Chem.* **112**, 321 (2012).
- ⁵ H. Isobe, M. Shoji, S. Yamanaka, Y. Umena, K. Kawakami, N. Kamiya, J.-R. Shen, and K. Yamaguchi, *Dalton Trans.* **41**, 13727 (2012).
- ⁶ T. Ichino, K. Yamaguchi, and Y. Yoshioka, *Chem. Lett.* **41**, 18 (2012).
- ⁷ K. Yamaguchi, S. Yamanaka, H. Isobe, T. Saito, K. Kanda, Y. Umena, K. Kawakami, J.-R. Shen, N. Kamiya, M. Okumura, H. Nakamura, M. Shoji, and Y. Yoshioka, *Int. J. Quantum Chem.* **113**, 453 (2013).
- ⁸ K. Yamaguchi, H. Isobe, S. Yamanaka, T. Saito, K. Kanda, M. Shoji, Y. Umena, K. Kawakami, J.-R. Shen, N. Kamiya, and M. Okumura, *Int. J. Quantum Chem.* **113**, 525 (2013).
- ⁹ P. E. Siegbahn, *ChemPhysChem* **12**, 3274 (2011).
- ¹⁰ P. E. Siegbahn, *Biochim. Biophys. Acta* **1827**, 1003 (2013).
- ¹¹ Y. Kurashige, G. K.-L. Chan, and T. Yanai, *Nat. Chem.* **5**, 660 (2013).
- ¹² K. Takatsuka, *J. Phys. Chem. A* **111**, 10196 (2007).
- ¹³ T. Yonehara and K. Takatsuka, *J. Chem. Phys.* **129**, 134109 (2008).
- ¹⁴ K. Takatsuka and T. Yonehara, *Adv. Chem. Phys.* **144**, 93 (2010).
- ¹⁵ T. Yonehara, K. Hanasaki, and K. Takatsuka, *Chem. Rev.* **112**, 499 (2011).
- ¹⁶ K. Yamamoto and K. Takatsuka, *J. Chem. Phys.* **140**, 124111 (2014).
- ¹⁷ M. W. Schmidt, K. K. Baldridge, J. A. Boatz, S. T. Elbert, M. S. Gordon, J. H. Jensen, S. Koseki, N. Matsunaga, K. A. Nguyen, S. Su, T. L. Windus, M. Dupuis, and J. A. Montgomery, *J. Comput. Chem.* **14**, 1347 (1993).
- ¹⁸ M. S. Gordon and M. W. Schmidt, *Theory and Applications of Computational Chemistry: the first forty years* (Elsevier, Amsteldam, 2005).
- ¹⁹ K. Nagashima and K. Takatsuka, *J. Phys. Chem. A* **116**, 11167 (2012).
- ²⁰ J. Paldus, *J. Chem. Phys.* **61**, 5321 (1974).
- ²¹ I. Shavitt, in *Methods of electronic structure theory* (Springer, 1977), pp. 189–275.
- ²² R. S. Mulliken, *J. Chem. Phys.* **23**, 1833 (1955).
- ²³ F. Hirshfeld, *Theor. Chim. Acta* **44**, 129 (1977).
- ²⁴ K. Takatsuka, T. Fueno, and K. Yamaguchi, *Theor. Chim. Acta* **48**, 175 (1978).
- ²⁵ L. I. Schiff, *Quantum mechanics* (McGraw-Hill, New York, 1968).
- ²⁶ M. Okuyama and K. Takatsuka, *Chem. Phys. Lett.* **476**, 109 (2009).
- ²⁷ K. Nagashima and K. Takatsuka, *J. Phys. Chem. A* **113**, 15240 (2009).
- ²⁸ M. Okuyama and K. Takatsuka, *Bull. Chem. Soc. Jpn.* **85**, 217 (2012).
- ²⁹ I. Barth, H.-C. Hege, H. Ikeda, A. Kenfack, M. Koppitz, J. Manz, F. Marquardt, and G. K. Paramonov, *Chem. Phys. Lett.* **481**, 118 (2009).
- ³⁰ J. Manz, J. F. Perez-Torres, and Y. Yang, *J. Phys. Chem. A* **118**, 8411 (2014).